ACS APPLIED MATERIALS & INTERFACES

Research Article

www.acsami.org

Gold–Oxoborate Nanocomposites and Their Biomedical Applications

Katarzyna Wybrańska,[†] Jan Paczesny,[†] Katarzyna Serejko,[†] Karolina Sura,[†] Karolina Włodyga,[†] Igor Dzięcielewski,[‡] Samuel T. Jones,[§] Agnieszka Śliwa,[⊥,#] Iwona Wybrańska,[∥,#] Robert Hołyst,[†] Oren A. Scherman,[§] and Marcin Fiałkowski*[,†]

[†]Institute of Physical Chemistry of the Polish Academy of Sciences, Kasprzaka 44/52, 01-224 Warsaw, Poland

[‡]Institute of High Pressure Physics of the Polish Academy of Sciences, Unipress, Sokołowska 29/37, 01-142 Warsaw, Poland

[§]Melville Laboratory for Polymer Synthesis, Department of Chemistry, University of Cambridge, Cambridge, CB2 1EW, U.K.

[∥]Department of Genetic Diagnostics and Nutrigenomics and [⊥]Department of Clinical Biochemistry, Medical College, Jagiellonian University, Kopernika 15a, 31-501 Cracow, Poland

[#]Malopolska Center of Biotechnology, Jagiellonian University, 30-387 Cracow, Poland

Supporting Information

ABSTRACT: A novel inorganic nanocomposite material, called BOA, which has the form of small building blocks composed of gold nanoparticles embedded in a polyoxoborate matrix, is presented. It is demonstrated that cotton wool decorated with the BOA nanocomposite displays strong antibacterial activity toward both Gram-positive and -negative bacteria strains. Importantly, the modified cotton does not release any toxic substances, and the bacteria are killed upon contact with the fibers coated with the BOA. Toxicity tests show that the nanocomposite—in spite of its antiseptic properties—is harmless for mammalian cells. The presented method of surface modification utilizes mild, environmentally friendly fabrication conditions. Thus, it offers a facile approach to obtain durable nontoxic antiseptic coatings for biomedical applications.

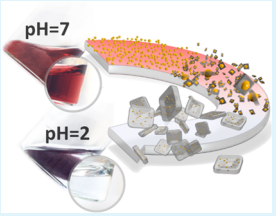

KEYWORDS: *antibacterial coating, cytotoxicity, nanocomposite, gold nanoparticles, oxoborates, surface modification*

1. INTRODUCTION

Nanocoatings are opening new opportunities in the area of surface modification, leading to novel applications in a variety of fields. Woven electronics,[1,2] self-cleaning surfaces,[3] antiseptic wound dressings and scaffolds,[4−6] conductive glass, and many more advanced inventions are being realized due to the development of novel nanocoatings. Nanoparticles were successfully incorporated into surface coatings that give rise to enhanced light resistance, improved mechanical and thermal performance, and moderate gas absorption of packaging for commercial use.[7] Nanocoatings capable of extinguishing flame on fabric have also been designed.[8] Some of the newly developed nanocoatings are already available on the market. Recently, the use of nanoparticles for the preparation of biofunctional coatings has been reported.[5,9−12] Nanoparticles embedded in a surface may act as antibacterial agents or sophisticated biosensors, or they can be employed as a carrier for controlled drug delivery.[13−15] Antibacterial coatings may also find use in the protection against biological or chemical weapons.[16]

There are still many uncertainties on how nanoparticles influence living organisms and the natural environment.[17] In particular, the mechanism of interaction of such nano-objects with living cells is diverse and very complex.[18,19] For instance, in a number of reports, the antibacterial properties of silver nanoparticles (AgNPs) are attributed to Ag^+ ion release.[20] At the same time, this mechanism is probably responsible for the toxicity of AgNPs against eukaryotic cells.[21] Gold nanoparticles (AuNPs) are proven to have antiseptic properties and they are also commonly believed to be nontoxic for mammalian cells.[22] However, it was shown that nanoparticles smaller than 12 nm in diameter may cross the blood–brain barrier, whereas those smaller than 30 nm can be endocytosed by cells.[20] Recent studies suggested that the AuNPs may cause cell damage by interacting with vital cell components such as the membrane, mitochondria, or nucleus.[15,24] The AuNPs exhibit different toxic activity, depending on their shape and size and the type of the cells.[23]

According to the latest report published by the European Centre For Disease Prevention and Control, one in 18 patients in European hospitals have at least one healthcare-associated infection. Overall, this amounts to an estimated total of 3.2 million patients each year. Thus, for biomedical applications it is highly desirable to design functional surfaces that are toxic for bacteria while being harmless to eukaryotic cells.[23,25,26] Here, to achieve this we immobilized AuNPs at the surface in a matrix of polyoxoborates to obtain surfaces that exhibit antibacterial activity based on the contact killing mechanism.[27−29] The main

Received: August 27, 2014
Accepted: January 27, 2015
Published: January 27, 2015

DOI: 10.1021/am508979y
ACS Appl. Mater. Interfaces 2015, 7, 3931−3939

advantage of our approach is the durability of the obtained polyoxoborates−AuNPs (BOA) nanocoating, which justifies the use of more expensive AuNPs rather than AgNPs. Moreover, nanocoatings with immobilized antibacterial agents exhibit reduced development of drug resistance and are regarded as being environmentally friendly.[30] Our method does not require any preconditioning steps, and the surface modification is carried out under mild conditions in aqueous solution. Our approach is based on the pH-dependent co-condensation of boric acid and oxoborate ions in the presence of the AuNPs. The resulting nanostructured material—referred to as the BOA nanocomposite—consists of building blocks that range in size from tens to hundreds of nanometers. BOA blocks are composed of AuNPs embedded in a polyoxoborate matrix. The BOA nanocomposite forms stable coatings that display high antibacterial activity against both Gram-negative and -positive bacteria, while being nontoxic for eukaryotic cells. We illustrate our method by applying it to the modification of cotton wool, the most commonly used material in biomedical applications.[31,32]

2. EXPERIMENTAL SECTION

2.1. Materials. $HAuCl_4 \cdot 3H_2O$ (99.8%, Aldrich), $NaBH_4$ granules (99%, Fluka, UK), HCl (analytical grade, POCH), NaOH (99.8%, POCH, Poland), H_2SO_4 (min 95%, POCH), H_2O_2 (30%, Chempur), and tetraethoxysilane (98%, Fluka) were used as received. Ethanol 96% (POCH) and chloroform (Chempur) used for cleaning were of analytical grade. Ultrapure water characterized by surface tension 72.75 mN m^{-1} at 20 °C and resistivity 18.2 MΩ cm was obtained from the Milli-Q water purification system. Silicon wafers were provided by the Institute of Electronic Materials Technology (Warsaw, Poland). Before use, the wafers were cleaned in a freshly prepared piranha solution [H_2SO_4:H_2O_2 = 7:3 (v/v)], rinsed several times with water, and dried under inert gas flow. Lysogeny broth (LB) liquid medium was purchased from Roth as an instant mix. Antibiotics were purchased from Sigma-Aldrich.

2.2. Synthesis and Characterization of Gold Nanoparticles. Gold nanoparticles (AuNP) were prepared according to the procedure described elsewhere.[33] Briefly, an aqueous stock solution of 50 mM gold chloride anions ($AuCl_4^-$) in a glass vial was prepared by dissolving $HAuCl_4 \cdot 3H_2O$ with the same molar amount of HCl. An aqueous solution of 50 mM borohydride anions (BH_4^-) in a glass vial was prepared by dissolving $NaBH_4$ with the same molar amount of NaOH, and 100 μL of $AuCl_4^-/H^+$ solution was added to a glass vial with 10 mL of deionized water. Afterward, 300 μL of BH_4^-/OH^- was added rapidly with stirring. The color of the solution turned from light yellow to brown-orange immediately and then to wine-red during further stirring. The average diameter of the AuNP core, determined from DLS and TEM studies, was 4.2 nm. The resulting concentration (2.2×10^{-7} M) of the colloidal solution of the AuNPs was calculated on the basis of the amount of reagents used for the synthesis and the mean diameter of the obtained particles.

2.3. Synthesis of SiO_2 Spheres. Submicrometric SiO_2 spheres were obtained via the Stöber method.[34] A 11.35 mL portion of ethanol and 0.65 mL of tetraethoxysilane (TEOS) were placed in a 20 mL glass bottle. The content of the bottle was stirred using a magnetic stirrer. Diluted ammonia solution was prepared by mixing 2 mL of 25% ammonia−water with 1 mL distilled water. The resulting ammonia solution was added to TEOS solution in ethanol. The solution became turbid 12 min after the solutions had been combined together, proving that the reaction was taking place. The reaction mixture was further stirred for 24 h. After that period, the resulting suspension was frozen out in a vacuum line to strip ethanol and ammonia. The resulting submicrometer particles (microspheres) were stored in an aqueous suspension of the same volume as the solution for the synthesis (15 mL).

2.4. Modification of Surfaces with the BOA. *2.4.1. Cotton Wool.* A 0.12 g portion of material was placed in a glass vial and 20 mL of the AuNP solution (2.2×10^{-7} M) was added. Then the pH was lowered to 2 by adding 300 μL of 0.5 M HCl, and the vial was shaken using a mechanical shaker (400 rpm) for ∼20 min to obtain uniform deposition.

2.4.2. Glass Fiber Fabric. A 5.5 × 5.0 cm^2 piece of material was placed in a glass vial, and 4 mL of the AuNP solution (2.2×10^{-7} M) was added. Next, the pH was lowered to 2 by adding 60 μL of 0.5 M HCl, and the vial was shaken using a mechanical shaker (400 rpm) for ∼30 min to obtain uniform deposition.

2.4.3. SiO_2 Microspheres. A 5 mL sample of the aqueous suspension of the microspheres obtained via the Stöber method was treated with HCl (1 M) to lower the pH to 2. Next, the sample was sonicated for 10 min, and 2 mL of the AuNP solution (2.2×10^{-7} M) was added. The samples were shaken (400 rpm) for 24 h. The modified microspheres had formed a red-violet precipitate.

All the modified materials (cotton wood, glass fiber, silica particles) were purified by repeated (three times) centrifugation (5 min, 5000 rpm), decantation of the solution from above the modified material, and replacement of the supernatant with pure deionized water (10 mL).

2.5. Tests of the Durability of the Coating (the "Washing Test"). A sample was placed in a plastic tube containing either ethanol, 2-propanol, chloroform, pure water, or an aqueous solution of a commercially available detergent [containing cocoamidopropyl betaine, coconut diethanolamide, cocamidopropylamine oxide, sodium 2-(2-dodecyloxyethoxy)ethyl sulfate, and sodium α-olefin sulfonate]. The sample was then shaken mechanically for 1 h at 400 rpm, dried under vacuum, and compared with the native modified cotton sample.

2.6. UV−Vis Measurements. Ultraviolet−visible absorbance spectra were recorded on Thermo Scientific Evolution 201 UV−vis spectrophotometer in the spectral range from 300 to 900 nm in 1 cm optical path glass cuvettes and in 0.5 cm optical path disposable sizing cuvettes (if applicable). Time-dependent measurements were performed with an Ocean-Optics USB 2000+ spectrophotometer in the spectral range 300−900 nm.

2.7. FTIR Measurements. The measurements were performed using a JASCO FTIR-6200 FTIR spectrophotometer (max resolution, 0.25 cm^{-1}; S/N ratio, 45 000:1; beam splitter, Ge/KBr) in the mid-IR region (4000−400 cm^{-1}). The standard technique with KBr pellets and an ATR-FTIR (attenuated total reflectance FTIR) method were utilized. Samples for the FTIR measurements were prepared as follows: AuNPs from colloidal solutions were precipitated by adding KBr (the "native" AuNPs) or 1 M HCl (BOA). The samples were then centrifuged (9000 rpm, 45 min), and the supernatant was removed. Prior to the measurements the precipitant was dried under vacuum overnight.

2.8. Raman Spectroscopy. Raman spectra of the BOA samples were measured using a Renishaw InVia Raman system equipped with a 300 mW diode laser emitting a 785 nm line as the excitation source. The light from the laser was passed through a line filter and focused on a sample mounted on an $X-Y-Z$ translation stage with a 10× microscope objective. The Raman scattered light was collected by the same objective through a holographic notch filter to block out Rayleigh scattering. A 1800 groove/mm grating was used to provide a spectral resolution of 5 cm^{-1}. The Raman scattering signal was recorded by a 1024 × 256 pixel RenCam CCD detector. The beam diameter was approximately 5 μm. Raman spectra were acquired for 20 min. Spectra were normalized by laser power and collection times. Samples for the Raman analysis were prepared by adding 300 μL of 0.5 M HCl to 20 mL of a colloidal solution of the AuNPs. A silicon plate was placed at the bottom of the vial. The supernatant was removed from the vial after the precipitation, and the silicon plate with adsorbed BOA aggregates was dried under vacuum overnight.

2.9. SEM and EDS Analysis. An ultrahigh resolution imaging microscope (Zeiss Ultra plus apparatus) was used to analyze the samples. The microscope was equipped with a microanalytical EDS (energy-dispersive X-ray spectroscopy) setup (Quantax 400 by

DOI: 10.1021/am508979y
ACS Appl. Mater. Interfaces 2015, 7, 3931−3939

Bruker) with an ultrafast (up to 300 kcounts/s) detector having a resolution of 127 eV and an active surface of 30 mm^2.

2.10. Surface Pressure Measurements and Brewster Angle Microscopy (BAM). Experiments were carried out using equipment from Nima Technology. The surface pressure sensor was detached from the Langmuir trough and mounted on an independent stand. The balance for surface pressure (π) measurements was of 0.05 mN m^{-1} resolution. A rectangular piece of analytical filtering paper (20 × 10 × 0.1 mm^3) was used as a surface pressure sensor. The sensor was calibrated before each experiment. A glass Petri dish 90 mm in diameter was used as the experimental vessel. Prior to every experiment the dishes were carefully cleaned with chloroform and ethanol and rinsed with water. The sensor was immersed in the solution of the AuNPs, and then HCl was added. In our experiments, 25 mL of the AuNPs solution was used. Then 380 μL of 0.5 M HCl was injected into the solution. The resulting pH was around 2.0. The surface pressure was monitored overnight. A Nanofilm Technology (MiniBAM) BAM microscope was used for in situ observations of the air−water interface. The system has a resolution of 8.3 μm per pixel. The field of observation was 4.8 × 6.4 mm^2. The experimental setup was placed in a polystyrene box to maintain the stability of the temperature and humidity of the atmosphere inside the box during the experiments. All experiments were performed at room temperature (23 °C).

2.11. DLS Measurements. The hydrodynamic radius of the BOA blocks in the solution was determined using a Zetasizer Nano ZS apparatus (Malvern Instruments Ltd.).

2.12. Bacteria Cultures and Viability Assays. *Escherichia coli* BL21(DE3) was used as an example of a Gram-negative bacteria. This bacteria strain was resistant to chloramphenicol and kanamycin. Green fluorescence protein (GFP) gene under control of the lac operon activated by addition of isopropyl-β-D-1-thiogalactopyranoside (IPTG) was present. Wild-type *Staphylococcus epidermidis* was investigated as a Gram-positive bacteria. Both Gram-positive and -negative bacteria were cultured according to the standard protocol. First, a single colony from an agar plate was inoculated into LB medium for overnight culturing (37 °C, 200 rpm). In the case of *E. coli*, chloramphenicol and kanamycin were added to final concentration of 50 μg mL^{-1}. The bacteria were cultured to obtain suspensions of OD_{600} = 1. Such a bacteria suspension was diluted 1000 times in saline solution and then divided into three portions. Control, unmodified cotton, and BOA-modified cotton samples were investigated. The same mass (0.036 g) of raw and the modified material was used. The colony forming units (cfu) counting method, after seeding 25 μL of bacteria suspensions onto agar plates, was used for determination of the microbial viability.

2.13. Eukaryotic Cell Culture Preparation and Cytotoxicity Test. 18LN neurons, BTC-6 pancreatic tumor, HepG2 hepatoma, and SVF progenitor stromal vascular fraction cells were studied. The cells were seeded in a 12-well flat bottom plates at a density of 10^5 cells/well for fluorescence microscopy studies and 2.5 × 10^5 cells/well in 500 μL of culture medium for LDH assay (see the Supporting Information for more details). In the latter experiment, samples in each experimental group were prepared in triplicate wells. All cells were cultured at 37 °C with 95% humidity and 5% CO_2.

The viability of cells incubated in a liquid media in the presence of BOA-modified cotton was observed under a Nikon ECLIPSE TS100 fluorescence microscope.

The cytotoxic effect of BOA-modified cotton was analyzed quantitatively by using a CytoTex 96 Non-Radioactive Cytotoxicity Assay (Promega) following the manufacturer's instructions.

3. RESULTS AND DISCUSSION

3.1. Preparation and Characterization of the BOA Nanocomposite Coating. The preparation and use of the antibacterial coatings based on the AuNPs need to address the following issues: (i) multistep, tedious procedures involving preconditioning of the substrate material and/or nanoparticles' ligand exchange;[27,35,36] (ii) the polydispersity of the AuNPs embedded on the surface, where nonuniformity can substantially impact the functionality of the coatings because the antiseptic activity of the AuNPs is dependent on their size;[23,37] (iii) the poor mechanical and chemical stability of the coating;[38] and (iv) the possible toxicity toward human tissues.[15,23,24] Below, we describe a protocol for the fabrication of an antibacterial coating containing nanostructured gold that does not suffer from these limitations.[39]

3.1.1. BOA Formation and Surface Modification Protocol. The protocol for modification of surfaces with the BOA nanocomposite according to our technique is illustrated in Figure 1a. The material to be modified is immersed in a solution containing AuNPs obtained via the Martin method.[33] Sodium borohydride used to synthesize the AuNPs fulfils two functions: (i) it acts as a reductive agent and (ii) it provides inorganic oxoborate ligands, which stabilize the AuNPs. The presence of the boron species, mainly in the form of boric acid, on the surface of the AuNPs was confirmed by IR spectroscopy studies [see sections 3.2.2 and 3.2.3 and the Supporting Information (SI)]. In our approach, $NaBH_4$ is also a source of

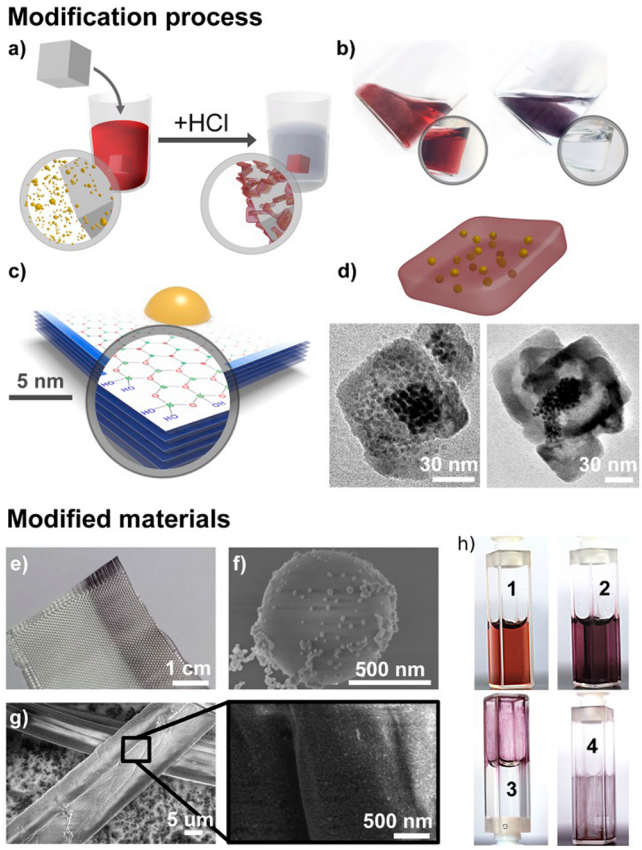

Figure 1. (a) Schematic representation of the surface modification procedure. (b) Initial and final stage of the cotton wool modification process: cotton in a solution of AuNPs before acidification with HCl (left) and modified cotton in supernatant (right). (c) Polyoxoborate ν-B_2O_3 matrix growing around a single AuNP. (d) TEM micrographs of the BOA blocks and schematic representation of their structure. (e) Digital picture of glass fiber fabric partially coated with the nanocomposite. SEM image of silica microparticles (f) and cotton fibers (g) covered with the BOA blocks. (h) Covering the glass surface with the nanocomposite: 1, glass cuvette with AuNP solution; 2, the same after the acidification; 3, BOA deposited on the walls of the cuvette, which is turned upside down to show that the postreaction solution is clear; 4, the cuvette after drying.

DOI: 10.1021/am508979y
ACS Appl. Mater. Interfaces 2015, 7, 3931−3939

the boron species that are needed to synthesize the BOA nanocomposite. The surface modification process is initiated by addition of a small amount of a 0.5 M solution of hydrogen chloride. After the acidification, the color of the solution changes instantaneously from red to violet, indicating the presence of structures in which the AuNPs are in close proximity. As revealed by transmission electron microscopy (TEM), UV−vis spectroscopy, and dynamic light scattering (DLS) studies (see SI), the BOA nanocomposite appears in the solution immediately after the acidification. Formation of the BOA nanostructures is followed by their deposition on the surface of the material being processed.

In our experiments, cotton wool, which is almost pure cellulose, was employed as the substrate material. Successful modification of cotton wool occurred at pH <7, but the highest efficiency—in terms of the adsorption rate and the total amount of the AuNPs adsorbed—was observed for pH ≤2. For such values of pH the modification process lasts about 30 min. It results in complete adsorption of the BOA nanocomposite on the surface of the substrate material, as evidenced by the fact that the supernatant solution becomes colorless and clear (Figure 1b). To examine the durability of the obtained coating, we performed a series of washing tests on the modified cotton wool, in which the samples were shaken vigorously for 1 h with water solutions containing detergent and with various organic solvents (see the SI). The samples did not stain the solutions and did not differ visually from the modified cotton wool that was not subjected to the test.

To demonstrate the versatility of the presented method, we successfully modified other hydrophilic substrates, such as fiberglass (Figure 1e), Stöber silica microspheres (Figure 1f), glass (Figure 1h), cotton fabric, and passivated silicon (see the SI). In each case, the surface modification process was carried out at room temperature and was completed within 20−60 min. Scanning electron microscopy (SEM) studies of the surface of the modified cotton and the Stöber spheres showed that the coating is composed of small (tens to hundreds of nanometers) nanocomposite blocks distributed uniformly over the surface (Figure 1g). Energy-dispersive X-ray spectroscopy (EDS) confirmed the presence of gold and boron atoms on the surface of the modified materials (Figure 2).

3.2. Formation of the BOA Nanocomposite. Formation of the BOA nanocomposite, accompanied by its adsorption on the surface of the material, is caused by the condensation of oxoborates under acidic condition.[40−43] For the boron concentrations used in our experiments (higher than 0.025 M), the borates coexist in the form of the nonionized acid, $B(OH)_3$, and polynuclear complexes $B_3O_3(OH)_4^-$, $B_4O_5(OH)_4^{2-}$, $B_3O_3(OH)_5^{2-}$, $B_5O_6(OH)_4^-$, and $B(OH)_4^-$.[42,44] Acidification of the solution leads to further condensation of the borates and formation of polyoxoborate structures. In an acidic medium, planar boric acid molecules tend to condense into sheetlike networks consisting of symmetrical boroxol rings.[45] IR combined with Raman spectroscopy studies confirmed the presence of the polyoxoborate structures composed of symmetrical hexagonal boroxol rings within the BOA nanocomposite (see also section 3.2.3 and the SI). The polymerization of the oxoborate anions causes charge delocalization and reduction of their formal charge.[42] As a consequence, the surface of the polyoxoborate sheetlike networks exhibits hydrophobic properties. The edges are hydrophilic, because of the presence of free OH groups. Stacking of such oxoborate sheets through hydrophobic forces

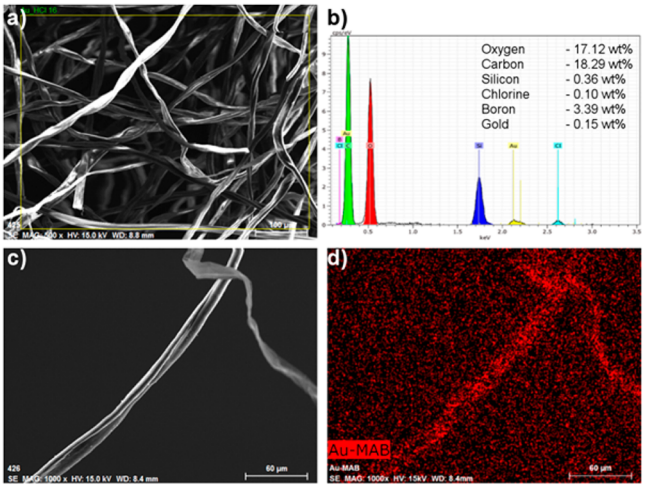

Figure 2. EDS-assisted SEM studies. SEM image of fibers of the cotton wool decorated with the BOA nanocomposite (a) and the distribution of the elements obtained with EDS (b). (c) SEM image of the modified cotton fibers along with the corresponding EDS map of the element gold (d).

and their further condensation mediated by the hydroxyl moieties give rise to the formation of the v-B_2O_3 matrix that exhibits amphiphilic properties. The top and bottom surfaces of the polyoxoborate matrix are hydrophobic, while its side faces are hydrophilic, because of the presence of free OH groups. Importantly, both the oxoborates of the stabilizing layers of the AuNPs and those present in the bulk solution are involved in the condensation reaction. Thus, at the early stages of the process, the v-B_2O_3 matrices are formed around the AuNPs. A schematic representation of such a hybrid AuNP−polyoxoborate structure is shown in Figure 1c. The AuNP−polyoxoborate hybrids further aggregate to assemble into the BOA blocks. This assembling process is driven by both the hydrophobic attraction and the condensation of the side hydroxyl groups. The shapes of the resulting BOA nanostructures, as revealed by TEM analysis (Figure 1d), can be approximated by square-based cuboids. An average length of their base edge is ∼80 nm. The nanocomposite blocks display a tendency to stack one on top of another. Such mutual arrangement indicates that the cuboids are flattened (that is, their height is smaller than the base edge length). TEM images suggest also that the central part of the block is thinner than the peripheries. Importantly, as evidenced by the TEM images, no aggregation of the AuNPs occurs during the condensation reaction, and the v-B_2O_3 matrices contain dispersed AuNPs. The structure of the BOA block, inferred from the TEM studies, is shown schematically in Figure 1d, along with the TEM images. The above scenario was confirmed by DLS and UV−vis measurements. We monitored the evolution of the sizes (hydrodynamic radii) of the structures formed after the acidification. Our studies showed that the formation of BOA blocks starts just after acid addition and that the size of the resulting blocks is several dozens of nanometers (<100 nm). Large objects (∼1 μm) appear after several minutes and they are assigned to the aggregating BOA blocks (see the SI for details). The condensation process was conducted in the absence of any supporting material in the solution.

The borate moieties present on the surface of the BOA blocks can undergo further condensation with free hydroxyl groups of cellulose (or other hydrophilic supporting materi-

DOI: 10.1021/am508979y
ACS Appl. Mater. Interfaces 2015, 7, 3931−3939

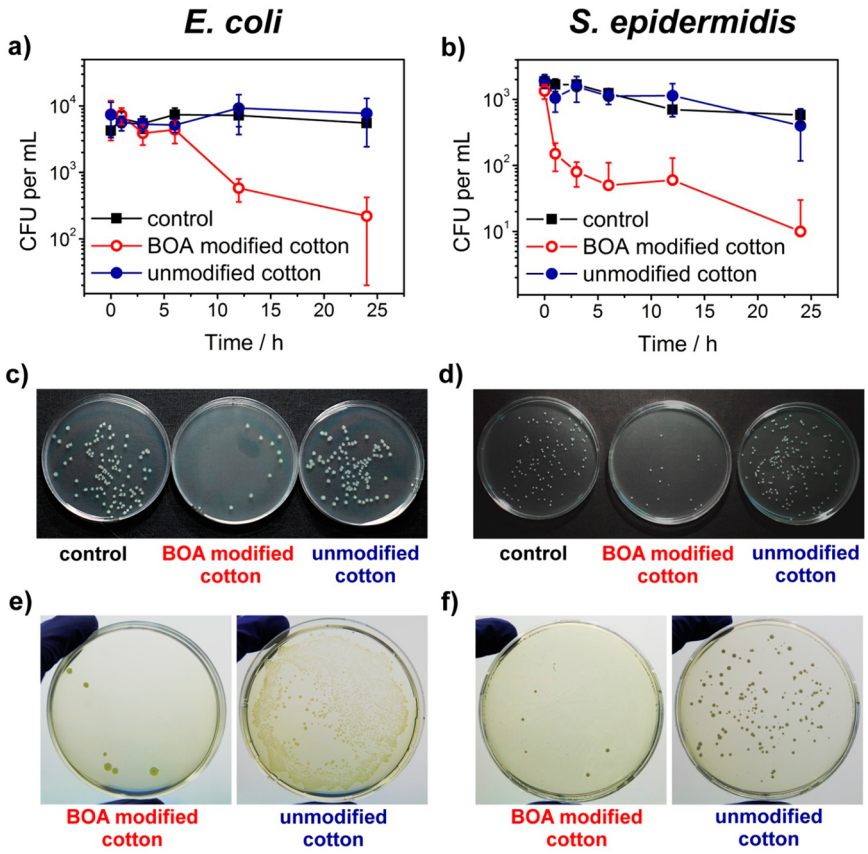

Figure 3. Antibacterial activity of the BOA. Bacterial survival curves for Gram-negative bacteria *E. coli* (a) and Gram-positive bacteria *S. epidermidis* (b) obtained with the colony counting method. Results of bacterial inoculations for *E. coli* (c) and *S. epidermidis* (d) observed for control and modified and raw cotton samples. Comparison of the bacterial inoculations from raw and modified cotton for *E. coli* (e) and *S. epidermidis* (f) on the agar plate.

al).[41] Consequently, the nanocomposite is covalently bonded to the substrate. We also found that in the absence of any material in the solution the BOA blocks display a tendency to accumulate and aggregate at the air−water interface. This observation is attributed to the amphiphilic nature of the BOA nanostructures discussed above. That is, for small nanocomposite assemblies the hydrophilic component of the surface (hydroxyl groups and the AuNPs) dominates. For large enough structures, the hydrophobic regions, located on the surfaces of the polyoxoborate sheets, prevail.

3.2.1. Surface Pressure Measurements and BAM Observations. The amphiphilicity of the BOA was further verified with the surface pressure, π, and Brewster angle microscopy (BAM) analysis. We observed that the fate of the AuNP upon addition of acid may be 2-fold: BOA nanocomposite can either adsorb on the surface of the modified material or—when there is no material to be modified—migrate to the air−water interface. We found (see Figure S8, SI) that π starts to grow shortly (~30 s) after the acidification of the AuNP solution. The increase of the surface pressure is caused by the hydrophobic nanocomposite blocks that migrate toward the air−water interface. BAM images presented in Figure S8 (SI) confirm the presence of the nanocomposite at the air−water interface.

3.2.2. IR Spectroscopy Analysis of AuNPs. Figure S2 (SI) shows the FTIR spectrum recorded for the native (precipitated with KBr) AuNPs samples. The FTIR absorption bands prove the presence of the borate groups at the surface of the investigated sample. Free boric acid exhibits one active band in the range of 1500−1300 cm^{-1} due to asymmetric stretching vibrations of B−O bonds (ν_3 mode) and very weak band in the range of 1100−950 cm^{-1} assigned to symmetric B−O stretching vibrations (ν_1 mode). If one proton of the boric acid is substituted with metal, then the symmetry of the molecule is lowered from D_{3h} to C_{2v}, which causes double degeneration of the asymmetric ν_3 band. Two peaks should be then be visible in the IR spectrum between 1250 and 1500 cm^{-1}. The symmetric stretch also becomes more infrared active, so there are a total of three B−O vibrations visible in a monodentate metal−boric acid complex. For bidentate metal−boric acid complexation, the symmetry remains C_{2v},[46] so the number of peaks does not change. The spectrum presented in Figure S2 (SI) displays the bands characteristic for the boric acid adsorbed to the metal surface: 1453 and 1376 cm^{-1} for ν_3 mode and 1101 cm^{-1} for ν_1 mode. Bands in the region 1000−1300 cm^{-1} are assigned to the bending vibrations within the plane of the B−O−H bonds (1164 and 1261 cm^{-1}),[46−49] indicating the presence of the $B(OH)_4^-$ ions. The broad band with a maximum at 3434 cm^{-1} characterizes stretching vibrations of the O−H bonds in the H_2O molecules adsorbed at the AuNP surface. The presence of the band assigned to the bending vibrations of H−O−H (1600 cm^{-1}) proves again that H_2O molecules are adsorbed on the AuNP surface.[50] The ATR-FTIR (attenuated total reflectance IR) spectrum of the native AuNPs is shown in Figure S3 (SI). The appearance of two bands located at 1456 and 1377 cm^{-1} provides further

DOI: 10.1021/am508979y
ACS Appl. Mater. Interfaces 2015, 7, 3931−3939

confirmation that the $B(OH)_3$ molecules are present on the surface of the AuNPs.

3.2.3. IR and Raman Spectroscopy Analysis of the BOA Nanocomposite. Figure S4 (SI) shows the FTIR spectrum recorded for BOA. The absence of any characteristic peak in the spectra indicates that boric acid polymerized into the *v*-B_2O_3 network that consists of symmetrical hexagonal boroxol rings. In such a network, the symmetric A_{1g} vibrations are strictly prohibited and are not detectable by IR spectroscopy. The presence of the *v*-B_2O_3 network was confirmed by Raman spectroscopy. The Raman spectrum recorded for the BOA sample is shown in Figure S5 (SI). The characteristic peak located at 807 cm^{-1} represents the symmetric breathing vibration of the boroxol ring. The broad band in the region 1300−1600 cm^{-1} in the Raman spectrum is assigned to the stretching of the nonbridging B−O bonds attached to large borate segments, such as metaborate rings, chain-type metaborate units, or triborate groups with one nonbridging oxygen.[51,52]

3.3. Antibacterial Activity of the BOA Nanocomposite Coating. *3.3.1. Quantitative Evaluation of the Antibacterial Activity of the BOA Nanocomposite.* We evaluated quantitatively the antibacterial activity of the BOA nanocomposite by investigating the bacteria viability of both Gram-negative and -positive bacteria incubated with the BOA-modified cotton. As a model of Gram-negative bacteria we used *E. coli* BL21(DE3) bacteria resistant to chloramphenicol and kanamycin. Wild-type *S. epidermidis* was used as an example of a Gram-positive strain. We studied the viability of bacteria cultured in LB liquid media by transferring them to saline solution containing either raw or the modified cotton samples. Viability curves obtained for *E. coli* and *S. epidermidis* are shown in parts a and b of Figure 3, respectively. In both cases, a significant decrease in the viability of the bacteria cultivated in the presence of BOA was observed. In terms of the cfu/mL, the viability of the bacteria exposed to the nanocomposite dropped within 24 h by at least 2 orders of magnitude compared to the control bacteria culture and the bacteria cultured with the unmodified cotton. Note that there was no difference in the viability between the control bacteria and the bacteria cultivated with unmodified cotton. Images of the bacterial inoculations on agar plates obtained for the control and modified and raw cotton samples after 24 h of cultivation time for *E. coli* and *S. epidermidis* are shown in parts c and d of Figure 3, respectively. In the second experiment, the bacteria (both *E. coli* and *S. epidermidis*) were cultured for 24 h in LB media containing the same amount of raw and modified cotton samples. Then, the samples were taken out and used for bacterial inoculation on agar plates (by pressing them against the surface of the plate). After incubation, the microbial viabilities of the bacteria present at the surface of the cotton samples were evaluated by cfu counting. Effects of the inoculations for both *E. coli* and *S. epidermidis* are shown in parts e and f of Figure 3, respectively. A substantial decrease of cfu number is observed for the modified material for both types of bacteria. This result confirms the strong antiseptic properties of the cotton fibers decorated with the BOA nanocomposite. More importantly, it rules out the possibility that the observed reduction of the microbial viability was due to the adsorption of the bacteria at the surface of the modified cotton.

3.3.2. Investigation of the Mechanism of Antibacterial Activity of BOA Nanocomposite. We performed also a series of experiments to explore the bacteria-killing mechanism. Cotton samples (0.0015 g) with six different amounts of BOA nanocomposite deposited were prepared. They were placed on Petri dishes on which *E. coli* bacteria were first inoculated. The Petri dishes were incubated at 37 °C for 48 h and then analyzed. We investigated six samples modified with BOA that were obtained under various conditions. The composition of the solutions used in the modification procedure for each sample is given in Table S1 (SI). Results of the experiments are shown in Figure S11 (SI). In each case, no visible zones of growth inhibition were observed. This suggests that the modified cotton is not releasing any toxic substances that may cause bacteria death.

To examine the antibacterial effect of the supernatant collected after the modification of the cotton fibers, we employed the Kirby−Bauer method. The dried surface of a Müller−Hinton agar plate was inoculated with a broth culture of *E. coli* bacteria diluted to match a 0.5 McFarland turbidity standard. After 5 min supernatant-impregnated disks were placed on the surface of the agar. Each disk was pressed down with forceps to ensure complete contact with the agar surface. The Petri dishes were incubated at 37 °C for 48 h and then analyzed. Results of the tests are presented in Figure 4. The

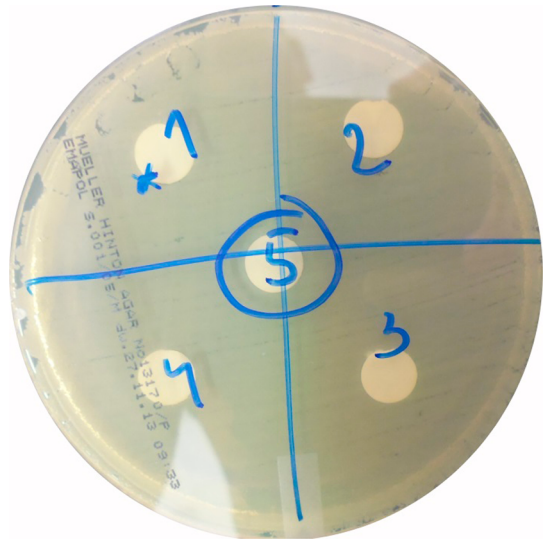

Figure 4. Results of Kirby−Bauer tests of the antibacterial activity of the supernatant collected from above the modified cotton fibers. Sample 1 corresponds to the supernatant collected directly after the modification. Samples 2, 3, 4, and 5 were collected after subsequent rinsing of the cotton with distilled water. None of the samples caused formation of a zone of inhibition around the filter-paper disks.

samples shown in Figure 4 correspond to the supernatant taken from above the cotton fibers immediately after the modification (sample 1) and after rinsing it with distilled water. The samples corresponding to the subsequent rinsing of the modified cotton are denoted as the samples 2, 3, 4, and 5. We found that none of the samples examined caused formation of the zone of inhibition around the filter-paper disks. This result provides an additional argument that there is no toxic substance released from the modified cotton.

Both of the experiments on the antibacterial activity of the supernatant described above prove that no antibacterial factor is released from the nanocomposite nor is present in the postreaction solution. Therefore, the bacteria are killed upon

DOI: 10.1021/am508979y
ACS Appl. Mater. Interfaces 2015, 7, 3931−3939

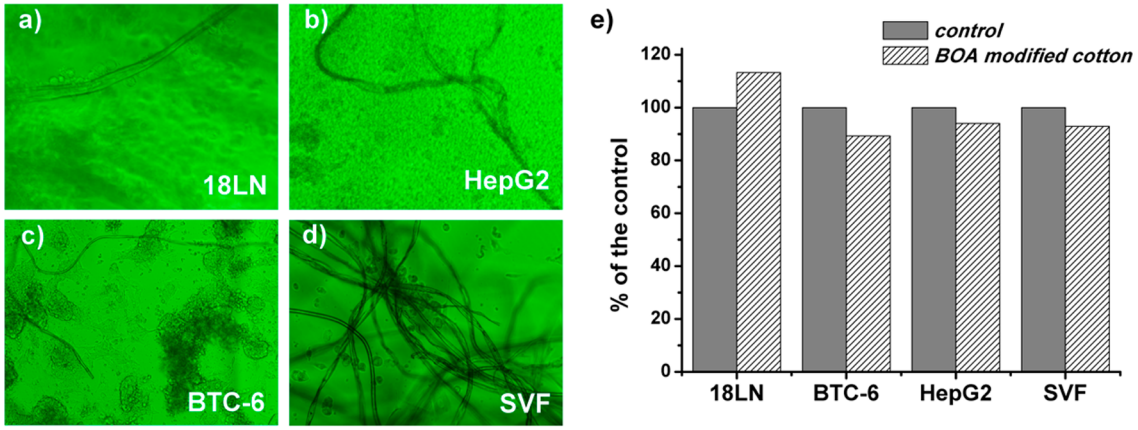

Figure 5. Demonstration of the nontoxicity of the nanocomposite to mammalian cells. Fluorescence microscope images of human cell cultures grown in the presence of the cotton wool coated with BOA: 18LN neurons (a), BTC-6 pancreatic tumor (b), HepG2 hepatoma (c), and SVF progenitor stromal vascular fraction (d) cells. Percentage of LDH activity, released into the medium after incubation with BOA-modified cotton, in comparison to the LDH activity in the negative control (without BOA-modified cotton) (e).

direct contact with the BOA and not due to ion release or nanoparticle uptake.[27−29]

We demonstrated that no other factors than the BOA nanocomposite (such as boric acid or other borate structures) are responsible for the antibacterial properties of the modified cotton. We studied the antibacterial activity of the cotton prepared using the same procedure, but without adding the AuNPs, and compared the obtained results to those of the BOA-modified cotton. The results of our experiments confirmed that the antibacterial activity is due to the presence of AuNPs in BOA nanocomposite. (see Figure S12 of the SI for more details).

3.4. Cytotoxicity of the BOA Nanocomposite Coating. Finally, we explored the toxic effects of the cotton wool modified with BOA toward mammalian cells. Four human cell lines were employed to evaluate the cytotoxicity of the nanocomposite: neurons (LN18), pancreatic islet cells (BTC-6), liver cells (HepG2), and stromal vascular fraction cells (SVF). The cells were grown in a liquid medium in the presence of the modified material (see the SI). Importantly, prior to testing, this material was not subjected to any disinfection procedures. The tests showed that all the cell lines can grow on the modified cotton in spite of its strong antiseptic properties. Remarkably, we found that not only in the presence of but also on the surface of the cotton fibers covered with BOA the cells could grow even 4 weeks after the inoculation. Representative images of the four cell lines cultivated in the presence of the modified cotton, observed under a fluorescence microscope, are shown in Figure 5a−d.

To quantify the effect of BOA on the cells, we used the LDH assay, which measures the lactate dehydrogenase (LDH) activity in the cell culture. The viability data shown in Figure 5e were calculated as the percentage of LDH activity released into the medium following the incubation with BOA-modified cotton. The data were related to the LDH activity in the negative control (without BOA modified cotton) that was taken as 100%. The examined samples were considered to be cytotoxic when the amount of LDH was increased by 20% when compared to the control. We did not see such an increase in the LDH activity in any experiment performed. The highest increase in LDH release (13% compared to the control) was observed for LN18 cells. This result demonstrates that the BOA coating is nontoxic for the human cell lines examined.

4. CONCLUSION

In summary, we presented the synthesis and characterization of a new inorganic nanostructured functional material, BOA, comprising gold nanoparticles and oxoborates. It has the form of small building blocks composed of gold nanoparticles embedded in a polyoxoborate matrix. These blocks have shapes of flattened square-based cuboids with a base edge length of a few tens of nanometers. Through the condensation reaction, the nanocomposite blocks can easily both self-assemble into three-dimensional aggregates or bind to various hydrophilic surfaces. We demonstrated that cotton wool decorated with the BOA nanocomposite displays strong antibacterial activity toward both Gram-positive and -negative bacteria strains. Importantly, the modified cotton is not releasing any toxic substances, and the bacteria are killed upon contact with the fibers coated with the BOA. Toxicity tests showed that—in spite of its antiseptic properties—the nanocomposite is harmless for mammalian cells. Finally, the method of surface modification we described uses mild, environmentally friendly fabrication conditions. Thus, it offers a facile approach to obtaining durable nontoxic antiseptic coatings for biomedical applications.

■ ASSOCIATED CONTENT

Ⓢ Supporting Information

Effect of pH on the surface coating fabrication, spectroscopic characterization of AuNPs and BOA nanocomposite, results of DLS and surface tension measurements, supplementary characterization of the antibacterial properties of the BOA coating, and experimental details of the cytotoxicity test. This material is available free of charge via the Internet at http://pubs.acs.org/.

■ AUTHOR INFORMATION

Corresponding Author

*E-mail: fialkows@ichf.edu.pl.

Author Contributions

The manuscript was written through contributions of all the authors. All authors have given approval to the final version of the manuscript. K.W. and J.P. contributed equally.

Notes

The authors declare no competing financial interest.

DOI: 10.1021/am508979y
ACS Appl. Mater. Interfaces 2015, 7, 3931−3939

■ ACKNOWLEDGMENTS

Project operated within the Foundation for Polish Science Team Programme cofinanced by the EU European Regional Development Fund, TEAM/2010-6/4. J.P. and K.W. acknowledge support of the National Science Centre within SONATA grant according to decision number 2012/07/D/ST5/02240; R.H. was supported by the National Science Centre Grant Opus 4 (UMO-2012/07/B/ST4/01400). The authors are grateful to A. Białecka and A. Kasprowicz from the Microbiological Research and Autovaccine Center in Kraków (CBMiA) for helpful discussions and performing some of the experiments with bacteria and A. Kamińska from IPC PAS for help with Raman spectroscopy measurements.

■ REFERENCES

(1) Lee, Y.; Kim, J.; Noh, J.; Lee, I.; Kim, H. J.; Choi, S.; Seo, J.; Jeon, S.; Kim, T.; Lee, J.; Choi, J. W. Wearable Textile Battery Rechargeable by Solar Energy. *ACS Nano Lett.* **2013**, *13*, 5753−5761.

(2) Zhong, J.; Zhang, Y.; Zhong, Q.; Hu, Q.; Hu, B.; Wang, Z. L.; Zhou, J. Fiber-Based Generator for Wearable Electronics and Mobile Medication. *ACS Nano* **2014**, *8*, 6273−6280.

(3) Hakim, L. F.; King, D. M.; Zhou, Y.; Gump, C. J.; George, S. M.; Weimer, A. W. Nanoparticle Coating for Advanced Optical, Mechanical and Rheological Properties. *Adv. Funct. Mater.* **2007**, *17*, 3175−3181.

(4) Wu, J.; Zheng, Y.; Wen, X.; Lin, Q.; Chen, X.; Wu, Z. Silver Nanoparticle/Bacterial Cellulose Gel Membranes for Antibacterial Wound Dressing: Investigation in Vitro and in Vivo. *Biomed. Mater.* **2014**, *9*, 1−12.

(5) Boonkaew, B.; Suwanpreuksa, P.; Cuttle, L.; Barber, P.; Supaphol, P. J. Hydrogels Containing Silver Nanoparticles for Burn Wounds Show Antimicrobial Activity without Cytotoxicity. *Appl. Polym. Sci.* **2014**, *131*, 1−10.

(6) Leaper, D. J. Silver Dressings: Their Role in Wound Management. *Int. Wound J.* **2006**, *3*, 282−294.

(7) Monteiro Cordeiro de Azeredo, H.; Capparelli Mattoso, L. H.; Habig McHugh, T. In *Advances in Diverse Industrial Applications of Nanocomposites*; Reddy, B. S. R., Ed.; InTech: Rijeka, Croatia, 2011; pp 57−78.

(8) Li, Y.-C.; Mannen, S.; Morgan, A. B.; Chang, S.; Yang, Y.-H.; Condon, B.; Grunlan, J. C. Intumescent All-Polymer Multilayer Nanocoating Capable of Extinguishing Flame on Fabric. *Adv. Mater.* **2011**, *23*, 3926−3931.

(9) Fleischer, S.; Shevach, M.; Feinerab, R.; Dvir, T. Coiled Fiber Scaffolds Embedded with Gold Nanoparticles Improve the Performance of Engineered Cardiac Tissues. *Nanoscale* **2014**, *6*, 9410−9414.

(10) Marsich, E.; Bellomo, F.; Turco, G.; Travan, A.; Donati, I.; Paoletti, S. Nano-composite Scaffolds for Bone Tissue Engineering Containing Silver Nanoparticles: Preparation, Characterization and Biological Properties. *J. Mater. Sci. Mater. Med.* **2013**, *24*, 1799−1807.

(11) Rizzello, L.; Cingolani, R.; Pompa, P. P. Nanotechnology Tools for Antibacterial Materials. *Nanomedicine (London)* **2013**, *8*, 807−821.

(12) Tscheliessnig, R.; Zörnig, M.; Herzig, E. M.; Lückerath, K.; Altrichter, J.; Kemter, K.; Paunel-Görgülü, A.; Lögters, T.; Windolff, J.; Pabischg, S.; Cinatl, J.; Rabenau, H. F.; Jungbauer, A.; Müller-Buschbaum, P.; Scholz, M.; Koch, J. Nano-Coating Protects Biofunctional Materials. *Mater. Today* **2012**, *15*, 394−404.

(13) Xue, C.-H.; Chen, J.; Yina, W.; Jia, S.-T.; Ma, J.-Z. Superhydrophobic Conductive Textiles With Antibacterial Property by Coating Fibers with Silver Nanoparticles. *Appl. Surf. Sci.* **2012**, *258*, 2468−2472.

(14) Guo, S.; Wang, E. Noble Metal Nanomaterials: Controllable Synthesis and Application in Fuel Cells and Analytical Sensors. *Nano Today* **2011**, *6*, 240−264.

(15) Sperling, R. A.; Rivera Gil, P.; Zhang, F.; Zanellaa, M.; Parak, W. J. Biological Applications of Gold Nanoparticles. *Chem. Soc. Rev.* **2008**, *37*, 1896−1908.

(16) Lee, S. B.; Koepsel, R. R.; Morley, S. W.; Matyjaszewski, K.; Sun, Y.; Russell, A. J. Permanent, Nonleaching Antibacterial Surfaces. 1. Synthesis by Atom Transfer Radical Polymerization. *Biomacromolecules* **2004**, *5*, 877−882.

(17) Geranio, L.; Heuberger, M.; Nowack, B. The Behavior of Silver Nanotextiles During Washing. *Environ. Sci. Technol.* **2009**, *43*, 8113−8118.

(18) Nel, A. E.; Mädler, L.; Velegol, D.; Xia, T.; Hoek, E. M. V.; Somasundaran, P.; Klaessig, F.; Castranova, V.; Thompson, M. Understanding Biophysicochemical Interactions at the Nano−Bio Interface. *Nat. Mater.* **2009**, *8*, 543−557.

(19) Conner, S. D.; Shmid, S. L. Regulated Portals of Entry Into the Cell. *Nature* **2003**, *422*, 37−44.

(20) Huda, S.; Smoukov, S. K.; Nakanishi, H.; Kowalczyk, B.; Bishop, K.; Grzybowski, B. A. Antibacterial Nanoparticle Monolayers Prepared on Chemically Inert Surfaces by Cooperative Electrostatic Adsorption (CELA). *ACS Appl. Mater. Interfaces* **2010**, *2*, 1206−1210.

(21) Knetsch, M. L. W.; Koolee, L. H. New Strategies in the Development of Antimicrobial Coatings: The Example of Increasing Usage of Silver and Silver Nanoparticles. *Polymers* **2011**, *3*, 340−366.

(22) Zhou, Y.; Kong, Y.; Kundu, S.; Cirillo, J. D.; Liang, H. Antibacterial Activities of Gold and Silver Nanoparticles Against *Escherichia coli* and Bacillus Calmette-Guérin. *J. Nanobiotechnol.* **2012**, *10*, 1−9.

(23) Murphy, C. J.; Gole, A. M.; Stone, J. W.; Sisco, P. N.; Alkilany, A. M.; Goldsmith, E. C.; Baxter, S. C. *Acc. Chem. Res.* **2008**, *41*, 1721.

(24) Alkilany, A. M.; Murphy, C. J. Toxicity and Cellular Uptake of Gold Nanoparticles: What We Have Learned so Far? *J. Nanopart. Res.* **2010**, *12*, 2313.

(25) Kim, S. T.; Saha, K.; Kim, C.; Rotello, V. M. The Role of Surface Functionality in Determining Nanoparticle Cytotoxicity. *Acc. Chem. Res.* **2013**, *46*, 681−91.

(26) Schwartz, V. B.; Thétiot, F.; Ritz, S.; Pütz, S.; Choritz, L.; Lappas, A.; Förch, R.; Landfester, K.; Jonas, U. Antibacterial Surface Coatings from Zinc Oxide Nanoparticles Embedded in Poly(*N*-isopropylacrylamide) Hydrogel Surface Layers. *Adv. Funct. Mater.* **2012**, *22*, 2376−2386.

(27) Cady, N. C.; Behnke, J. L.; Strickland, A. D. Copper-Based Nanostructured Coatings on Natural Cellulose: Nanocomposites Exhibiting Rapid and Efficient Inhibition of a Multi-Drug Resistant Wound Pathogen, *A. baumannii*, and Mammalian Cell Biocompatibility in Vitro. *Adv. Funct. Mater.* **2011**, *21*, 2506−2514.

(28) Pang, H.; Gao, F.; Lu, Q. Morphology Effect on Antibacterial Activity of Cuprous Oxide. *Chem. Commun.* **2009**, *9*, 1076−1078.

(29) Lichter, J. A.; Rubner, M. F. Polyelectrolyte Multilayers with Intrinsic Antimicrobial Functionality: The Importance of Mobile Polycations. *Langmuir* **2009**, *25*, 7686−7694.

(30) Li, Z.; Lee, D.; Sheng, X.; Cohen, R. E.; Rubner, M. F. Two-Level Antibacterial Coating with Both Release-Killing and Contact-Killing Capabilities. *Langmuir* **2006**, *22*, 9820−9823.

(31) Hoenich, N. Cellulose for Medical Applications: Past, Present, and Future. *BioResources* **2006**, *1*, 270−280.

(32) Mohanty, A. K.; Misra, M.; Drzal, L. T. Sustainable Bio-Composites from Renewable Resources: Opportunities and Challenges in the Green Materials World. *J. Polym. Environ.* **2002**, *10*, 19−26.

(33) Martin, M. N.; Basham, J. I.; Chando, P.; Eah, S. Charged Gold Nanoparticles in Non-Polar Solvents: 10-min Synthesis and 2D Self-Assembly. *Langmuir* **2010**, *26*, 7410−7417.

(34) Stöber, W.; Fink, A.; Bohn, E. Controlled Growth of Monodisperse Silica Spheres in the Micron Size Range. *J. Colloid Interface Sci.* **1968**, *26*, 62−69.

(35) Sosibo, N.; Mdluli, P.; Mashazi, P.; Tshikhudo, R.; Skepu, A.; Vilakazi, S.; Nyokong, T. Facile Deposition of Gold Nanoparticle Thin Films on Semi-Permeable Cellulose Substrate. *Mater. Lett.* **2012**, *88*, 132−135.

(36) Dong, H.; Hinestroza, J. P. Metal Nanoparticles on Natural Cellulose Fibers: Electrostatic Assembly and in Situ Synthesis. *ACS Appl. Mater. Interfaces* **2009**, *1*, 797−803.

DOI: 10.1021/am508979y
ACS Appl. Mater. Interfaces 2015, 7, 3931−3939

(37) Guo, L.; Yuan, W.; Lu, Z.; Li, C.-M. Polymer/Nanosilver Composite Coatings for Antibacterial Applications. *Colloids Surf., A* **2013**, *439*, 69−83.
(38) Pinto, R. J. B.; Marques, P. A. A. P.; Martins, M. A.; Neto, C. P.; Trindade, T. Electrostatic Assembly and Growth of Gold Nanoparticles in Cellulosic Fibres. *J. Colloid Interface Sci.* **2007**, *312*, 506−512.
(39) Wybrańska, K.; Paczesny, J.; Hołyst, R.; Fiałkowski, M. PCT Patent Application 075709, 2013.
(40) Zhihong, L.; Bo, G.; Shuni, L.; Mancheng, H.; Shuping, X. Raman Spectroscopic Analysis of Supersaturated Aqueous Solution of $MgO{\cdot}B_2O_3$−32%$MgCl_2$−H_2O during Acidification and Dilution. *Spectrochim. Acta, Part A* **2004**, *60*, 3125−3128.
(41) Bishop, M.; Shahid, N.; Yang, J.; Barron, A. R. Determination of the Mode and Efficacy of the Cross-Linking of Guar by Borate Using MAS 11B NMR of Borate Cross-linked Guar in Combination with Solution ^{11}B NMR of Model Systems. *Dalton Trans.* **2004**, *17*, 2621−2634.
(42) Leonyuk, N. J. In *Contemporary Boron Chemistry*; Davidson, M. G., Wade, K., Marder, T. B., Hughes, A. K., Eds.; Royal Society of Chemistry: London, 2000; pp 96−98.
(43) Feigl, F. *Specific and Special Reactions for Use in Qualitative Analysis: With Particular Reference to Spot Test Analysis*, 3d ed.; Nordemann: New York, 1940.
(44) Farmer, J. B. In *Advances In Inorganic Chemistry*; Emeléus, H. J., Sharpe, A. G., Eds.; Elsevier: New York, 1982; Vol. *25*, pp 187−225.
(45) Lin, Z.-E.; Yang, G.-Y. Oxo Boron Clusters and Their Open Frameworks. *Eur. J. Inorg. Chem.* **2011**, *26*, 3857−3867.
(46) Peak, D.; Luther, G. W.; Sparks, D. L. ATR-FTIR Spectroscopic Studies of Boric Acid Adsorption on Hydrous Ferric Oxide. *Geochim. Cosmochim. Acta* **2003**, *67*, 2551−2560.
(47) Markowa-Deneva, I. Infrared Spectroscopy Investigation of Metallic Nanoparticles Based on Copper, Cobalt and Nickel Synthesized through Borohydride Reduction Method. *J. Univ. Chem. Technol. Metall.* **2010**, *45*, 351−378.
(48) Su, C.; Suarez, D. L. Coordination of Adsorbed Boron: A FTIR Spectroscopic Study. *Environ. Sci. Technol.* **1995**, *29*, 302−311.
(49) Kamitsos, E. I.; Chryssikos, G. D. Borate Glass Structure by Raman and Infrared Spectroscopies. *J. Mol. Struct.* **1991**, *247*, 1−16.
(50) Melendres, C. A.; Beden, J. B.; Bowmaker, G.; Liu, C.; Maroni, V. A. Synchrotron Infrared Spectroscopy of H_2O Adsorbed on Polycrystalline Gold. *Langmuir* **1993**, *9*, 1980−1982.
(51) Ram, S. Infrared Study of the Dynamics of Boroxol Rings in the Crystallization of $BaFe_{12}O_9$ Microcrystals in Borate Glasses. *Phys. Rev. B* **1995**, *51*, 6280−6286.
(52) Bril, T. W. Ph.D. Dissertation, Technische Hogeschool, Eindhoven, Netherlands, 1976.

DOI: 10.1021/am508979y
ACS Appl. Mater. Interfaces 2015, 7, 3931−3939